Supplemental Document

Wavelength-scale optical parametric oscillators: supplement

SAMAN JAHANI, ARKADEV ROY, AND ALIREZA MARANDI*

Department of Electrical Engineering, California Institute of Technology, Pasadena, California 91125, USA
**Corresponding author: marandi@caltech.edu*

Supplement DOI: https://doi.org/10.6084/m9.figshare.13611461

Parent Article DOI: https://doi.org/10.1364/OPTICA.411708

Wavelength-scale optical parametric oscillators: supplementary material

SAMAN JAHANI[1], ARKADEV ROY[1], AND ALIREZA MARANDI[1,*]

[1] *Department of Electrical Engineering, California Institute of Technology, Pasadena, CA 91125, USA*
[*] *Corresponding author: marandi@caltech.edu*

Compiled December 11, 2020

In the Supplementary Material, we derive the equations for single-mode and multi-mode OPOs for both degenerate and non-degenerate cases. We derive the second-harmonic generation (SHG) efficiency and establish a connection between the SHG efficiency and the threshold in degenerate OPOs for single mode cases. We discuss the quasi-normal modes for dispersive and non-spherical cases and the role of low-Q background modes on the performance of arbitrarily-shaped OPOs. We provide more details on the parameters, eigenvalues and eigenvectors of the results displayed in the main text.

1. WAVE EQUATIONS

The Helmholtz wave equation in presence of nonlinear polarizability can be written as:

$$\begin{aligned}\nabla^2\vec{E} &= \mu_0\frac{\partial}{\partial t}\left(\frac{\partial\vec{D}}{\partial t}+\sigma\vec{E}\right) \\ &= \mu_0\varepsilon_0\varepsilon\frac{\partial^2\vec{E}}{\partial t^2}+\mu_0\sigma\frac{\partial\vec{E}}{\partial t}+\mu_0\frac{\partial^2\vec{P}_{\mathrm{NL}}}{\partial t^2},\end{aligned} \tag{1}$$

where $\varepsilon = n^2$ is the linear relative permittivity, n is the refractive index, and P_{NL} is the nonlinear polarization. To describe nonlinear dynamics in wavelength-scale cavities, we write the electric field as a superposition of the cavity eigenmodes. Instead of the conventional form of spatial SVEA in which the envelope evolves as the wave propagates through the nonlinear medium, we assume that the envelope is stationary in space but slowly evolves in time:

$$\begin{aligned}\vec{E}(\vec{r},t) &= \mathcal{E}_a\sum_k a_k(t)e^{-i(\omega-i\frac{\alpha_k}{2})t}|\vec{\psi}_k(\vec{r})\rangle + c.c., \\ \vec{P}_{\mathrm{NL}}(\vec{r},t) &= \sum_k \vec{P}_k(\vec{r},t)e^{-i(\omega-i\frac{\alpha_k}{2})t} + c.c.,\end{aligned} \tag{2}$$

where $\mathcal{E}_a$ is the normalization constant such that $|a_k|^2$ is the energy stored in the kth mode of the cavity, and for a homogeneous resonator, it is $\mathcal{E}_a = \sqrt{2/\varepsilon_0 n(\omega)^2}$, $\vec{P}_k$ is the nonlinear polarization that we explain later, $|\vec{\psi}_k(\vec{r})\rangle$ is the cavity eigenmode normalized such that $\langle\vec{\psi}_m(\vec{r})\vec{\psi}_k(\vec{r})\rangle = \delta_{mk}$ (δ_{mk} is the Kronecker delta), ω is the angular frequency of the signal, idler or pump, $\alpha_k = \omega_k/Q_k$ is the decay rate of the cavity mode, ω_k is the eigenfrequency of the k-th mode with a quality factor of Q_k.

In the following, we first formulate the nonlinear dynamics for a single-mode OPO at degeneracy, and then we expand the formalism to a multi-mode cavity and non-degenerate case.

By inserting Eq. 2 in to Eq. 1, considering the kth mode is the only mode at the operating frequency, we have:

$$\begin{aligned}&\{\nabla^2+\frac{\omega^2}{c^2}n^2-\frac{n^2}{c^2}\frac{\partial^2}{\partial t^2}+\frac{2i\left(\omega-i\frac{\alpha_k}{2}\right)}{c^2}n^2\frac{\partial}{\partial t} \\ &+\frac{i\alpha_k\omega-\alpha_k^2/4}{c^2}n^2+i\omega\mu_0\sigma+\mu_0\sigma\frac{\partial}{\partial t}\}\mathcal{E}_a a_k(t)|\vec{\psi}_k(\vec{r})\rangle \\ &= -\mu_0\left(\omega-i\frac{\alpha_k}{2}\right)^2\vec{P}_k+2i\mu_0\left(\omega-i\frac{\alpha_k}{2}\right)\frac{\partial\vec{P}_k}{\partial t}+\mu_0\frac{\partial^2\vec{P}_k}{\partial t^2}.\end{aligned} \tag{3}$$

Because of SVEA, $\omega \gg \alpha_k$, $\omega P_k \gg \frac{\partial P_k}{\partial t}$, and $\omega a_k \gg \frac{\partial a_k}{\partial t}$. Also, if we ignore the effect of the nonlinearity on the dispersion and if we assume that $\omega = \omega_k + \delta\omega_k$ where $\omega_k \gg \delta\omega_k$, we can assume $\left(\nabla^2+\frac{\omega_k^2}{c^2}n^2\right)|\vec{\psi}_k(\vec{r})\rangle \approx 0$. With these approximations, the wave equation is simplified to:

$$\begin{aligned}&\{\frac{2i\omega n^2}{c^2}\frac{\partial}{\partial t}+i\omega\mu_0\sigma a_k \\ &+\frac{(2\delta\omega_k+i\alpha_k)\omega n^2}{c^2}\}\mathcal{E}_a a_k(t)|\vec{\psi}_k(\vec{r})\rangle = -\mu_0\omega^2\vec{P}_k.\end{aligned} \tag{4}$$

Dividing the both sides by $2i\omega n^2/c^2$, we reach:

$$\{\frac{\partial}{\partial t}+\frac{\mu_0\sigma c^2}{2}-i\delta\omega_k+\frac{\alpha_k}{2}\}\mathcal{E}_a a_k(t)|\vec{\psi}_k(\vec{r})\rangle=\frac{i\mu_0\omega c^2}{2n^2}\vec{P}_k. \quad (5)$$

Note that we have assumed a weak material dispersion to derive the above equation. For dispersive structures, the evolution of modes need more rigorous analysis [1]. We first implement the nonlinear dynamics to estimate the threshold in single-mode OPOs. Then, we extend our model when the cavity has multiple modes at the signal wavelength. We also applies our model for second-harmonic generation, we show that if the second-harmonic signal is single-mode, we can estimate the threshold from SHG efficiency. This can be helpful to estimate the OPO threshold for the structures which have already been proposed for SHG.

2. HALF-HARMONIC GENERATION

By writing the nonlinear polarization, we can find the nonlinear dynamics for different nonlinear processes (e.g. second-harmonic generation and half-harmonic generation). Here, we first focus on the threshold for half-harmonic generation in degenerate OPOs. For simplicity, we ignore the ohmic loss of the modes.

The coupled nonlinear wave equation for signal and pump can be written as:

$$\sum_k\{\frac{\partial}{\partial t}-i\delta\omega_k^{(a)}+\frac{\alpha_k^{(a)}}{2}\}a_k(t)|\vec{\psi}_k^{(a)}(\vec{r})\rangle \quad (6)$$
$$=\sum_k\frac{i\omega}{2n(\omega)^2}\chi^{(2)}(2\omega,\omega,\omega)\mathcal{E}_b b(t)a_k^*(t)|\vec{\Psi}^{(b)}(\vec{r})|\vec{\psi}_k^{(a)^*}(\vec{r})\rangle,$$

$$\{\frac{\partial}{\partial t}-i\delta\omega^{(b)}+\frac{\alpha^{(b)}}{2}\}b(t)|\vec{\Psi}^{(b)}(\vec{r})\rangle \quad (7)$$
$$=\sum_k\frac{i\omega}{n(2\omega)^2}\chi^{(2)}(2\omega,\omega,\omega)\frac{\mathcal{E}_a^2}{\mathcal{E}_b}a_k^2(t)|\vec{\psi}_k^{(a)^2}(\vec{r})\rangle.$$

We have defined the electric field for the signal at the fundamental harmonic as $\vec{E}_\omega=\mathcal{E}_a\sum a_k(t)e^{-i(\omega-i\frac{1}{2}\alpha_k^{(a)})t}|\vec{\psi}_k^{(a)}(\vec{r})\rangle$, where $|\vec{\psi}_k^{(a)}(\vec{r})\rangle$ are the eigenmodes of the cavity at $\omega=\omega_k$ with decay constant of $\alpha_k^{(a)}$. The electric field for the pump at second-harmonic is defined as $\vec{E}_{2\omega}=\mathcal{E}_b e^{-i(2\omega-\frac{1}{2}\alpha^{(b)})t}b(t)|\vec{\Psi}^{(b)}(\vec{r})\rangle$, where $|\vec{\Psi}^{(b)}(\vec{r})\rangle$ is the spatial mode profile of the pump normalized such that $\langle\vec{\Psi}^{(b)}(\vec{r})\vec{\Psi}^{(b)}(\vec{r})\rangle=1$ but, as we explain later, it does not have to be the eigenmode of the cavity and it can be an embedded eigenmode of the cavity, such as Fano, anapole, or bound-state in the continuum modes, $b(t)$ is the envelope of the pump such that $|b|^2$ is the pump power, and $\alpha^{(b)}$ is the decay rate for the pump mode.

A. Single-mode cavity

If $|\vec{\psi}_k^{(a)}(\vec{r})\rangle$ is the only mode of the cavity at the operating frequency, by multiplying the both sides of Eqs. 6 and 7 by $\langle\vec{\psi}_k^{(a)}(\vec{r})|$ and $\langle\vec{\Psi}^{(b)}(\vec{r})|$, respectively, and calculating the inner product, the coupled equations are simplified to:

$$\frac{d}{dt}a_k=\left(i\delta\omega_k^{(a)}-\frac{\alpha_k^{(a)}}{2}\right)a_k+i\eta_{kk}ba_k^*, \quad (8)$$

$$\frac{d}{dt}b=\left(i\delta\omega^{(b)}-\frac{\alpha^{(b)}}{2}\right)(b-b_0)+i2\eta_{kk}^*a_k^2, \quad (9)$$

where b_0 is the pump amplitude in the absence of the nonlinearity and η_{lk} is the effective nonlinear coupling defined as:

$$\eta_{lk}=\omega\langle\frac{\mathcal{E}_b\chi^{(2)}}{n(\omega)^2}\vec{\psi}_l^{(a)^*}(\vec{r})\vec{\Psi}^{(b)}(\vec{r})\vec{\psi}_k^{(a)^*}(\vec{r})\rangle. \quad (10)$$

Near the OPO threshold, we can assume that the pump is not depleted ($b=b_0$). Above threshold, Eqs. 8 and 9 must be solved simultaneously. The steady-state amplitude of the signal is the solution of Eq. 8 when $da_k/dt=0$. There are two solutions: one of them is the trivial solution, $a_k=0$, which represents the OPO below the threshold; the nontrivial solution which represents the OPO at threshold. This requires that the amplitude and phase of the pump satisfy these conditions:

$$|\eta_{kk}b_0|\sin(\phi_b-2\phi_k)=\frac{\alpha_k^{(a)}}{2}, \quad (11)$$
$$|\eta_{kk}b_0|\cos(\phi_b-2\phi_k)=-\delta\omega_k^{(a)},$$

where ϕ_k and ϕ_b are the phase of the signal mode and the pump mode, respectively. As far as the threshold power is concerned, the above equation can be written in a more compact form [2, 3]:

$$|b_0|^2=\frac{1}{|\eta_{kk}|^2}\left(\frac{{\alpha_k^{(a)}}^2}{4}+{\delta\omega_k^{(a)}}^2\right). \quad (12)$$

If there is only one coupling channel between the input source and the cavity mode at the pump frequency, in the weak coupling regime ($Q_k\gg1$), the coupling between the input source and the pump cavity mode in the steady-state can be written as [3]:

$$|b_0|^2=\frac{\alpha^{(b)}}{\frac{{\alpha^{(b)}}^2}{4}+{\delta\omega^{(b)}}^2}P_{\text{in}}. \quad (13)$$

Hence, the threshold for the input source to go above threshold is:

$$P_{\text{th}}=\frac{1}{\alpha^{(b)}|\eta_{kk}|^2}\left(\frac{{\alpha_k^{(a)}}^2}{4}+{\delta\omega_k^{(a)}}^2\right)\left(\frac{{\alpha^{(b)}}^2}{4}+{\delta\omega^{(b)}}^2\right). \quad (14)$$

If there are more than one coupling channel between the input and the cavity, such as the excitation from the free-space, Eq. 14 is not accurate, and the coupling between the input power and the pump mode amplitude, b_0, should be derived from the linear analysis of the cavity at the pump frequency.

B. Multi-mode cavity

For wavelength-scale cavities, the quality factor of the modes are usually low. Hence, at operating wavelength more than one can resonate. If the cavity is multi-mode at the operating wavelength, by multiplying the both sides of Eq. 6 by $\langle\vec{\psi}_l^{(a)}(\vec{r})$, the coupled equation is simplified to:

$$\frac{d}{dt}a_l=\left(i\delta\omega_l^{(a)}-\frac{\alpha_l^{(a)}}{2}\right)a_l+ib\sum_k\eta_{lk}a_k^*. \quad (15)$$

The steady-state response of this equation can be written in a matrix form as:

$$\boldsymbol{\mathcal{H}}(b)\left[a_1,a_1^*,...,a_k,a_k^*,...\right]^T=0. \quad (16)$$

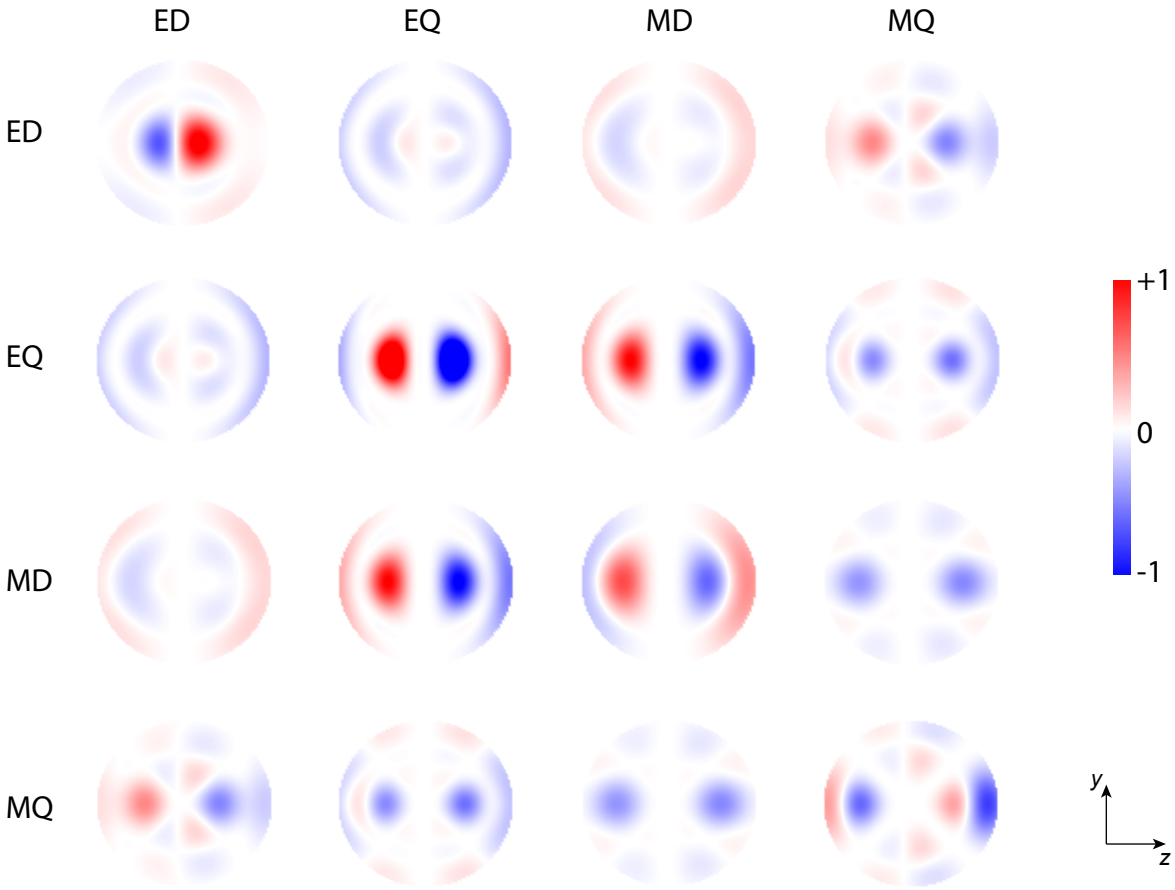

Fig. 1. Field overlap between the pump, signal, and idler. Normalized local field overlap, which is defined in Eq. 10, between the pump (for the structure shown in Fig. 3 in the main text when the pump is resonating at the 3rd magnetic mode), signal (rows), and idler (columns) modes in the nonlinear region. The integration of the overlap leads to the nonlinear coupling matrix demonstrated in Eq. 26. It is seen that even though the intensity of local overlap for some modes are high, the nonlinear coupling is small due to the weak overlap between the mode profiles. This means that increasing the field intensity locally (e.g. by increasing the Q factor) does not always lead to a stronger nonlinear response in wavelength-scale resonators.

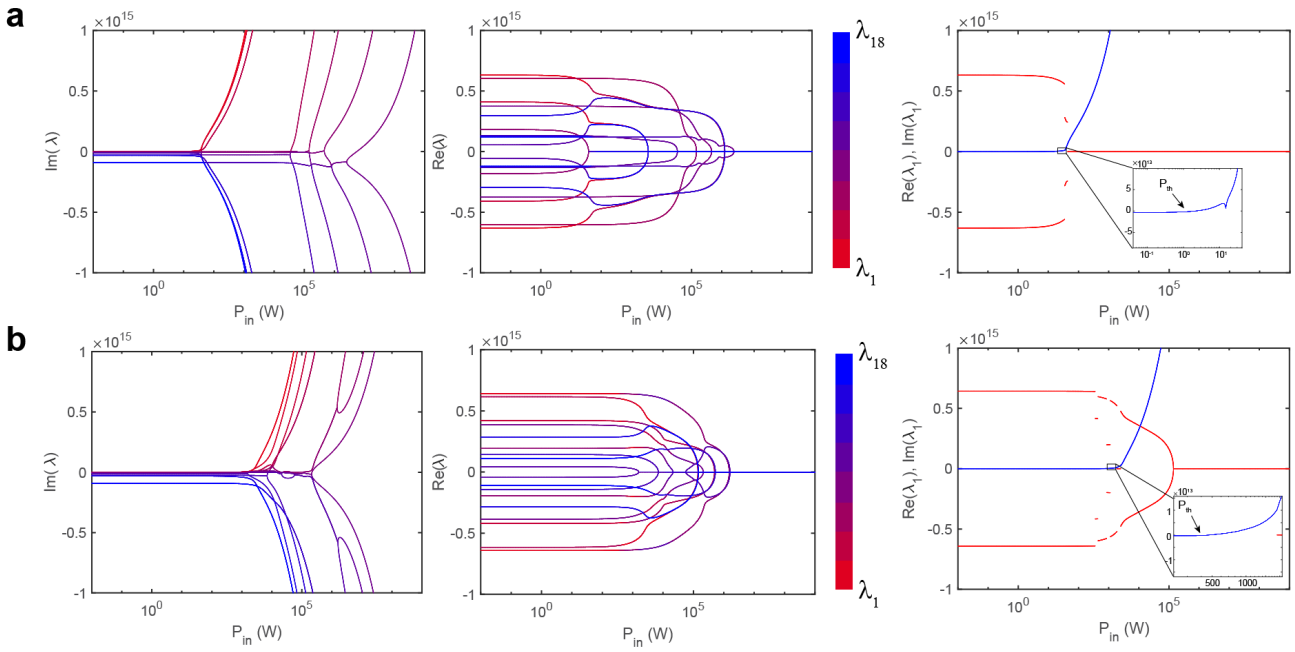

Fig. 2. Eigenvalues of the wavelength-scale OPOs. The structure is the same as that Fin. 6 in the main text. **a,** the pump wavelength is at 1110 nm. **b,** the pump wavelength is at 1125 nm. The OPO threshold is 2W and 467 W, respectively. However, the parametric gain is small because of the large signal/idler separation. As soon as the OPO goes through a phase transition into degenerate phase, the parametric gain increases rapidly. The threshold for degenerate OPO is 34 W and 1929 W, respectively.

The OPO threshold is the minimum pump power for which the determinant of the matrix passes zero. Near the threshold, that is the only oscillating mode and the eigenvector correspond to that eigenvector describes the spatial distribution of the signal. The phase difference between each mode of the pulse and the pump is set automatically to achieve the minimum threshold. There is no closed form solution for the eigenvalue if the quality factors of the modes or the central frequencies of all modes are not the same. However, in the best case scenario where all the modes have similar nonlinear coupling coefficient and quality factor, the threshold is reduced by a factor which is the number of modes.

As seen in Figs. 3 and 6 in the main text, the threshold for degenerate OPO is not always lower than the non-degenerate case. Hence, it is crucial to consider non-degenerate cases as well.

If signal and idler modes are non-degenerate, Eq. 15 is changed to:

$$\frac{d}{dt}a_l^{(s)} = \left(i\delta\omega_l^{(a)} - \frac{\alpha_l^{(a)}}{2}\right)a_l^{(s)} + ib\sum_k \eta_{lk}a_k^{(i)*}, \tag{17}$$

where $a_l^{(s)}$ and $a_l^{(s)}$, represent the envelope of the l^{th} signal and idler mode, respectively. In this case, the eigenvalues are not necessarily real, and the steady-state response can be oscillatory. As a result, the eigenvalue problem of Eq. 16 is changed to:

$$\frac{d}{dt}\boldsymbol{\mathcal{A}}(t) = \boldsymbol{\mathcal{H}}(b)\boldsymbol{\mathcal{A}}(t) \tag{18}$$

where $\boldsymbol{\mathcal{A}}(t) = \left[a_1^{(s)}, a_1^{(i)*}, ..., a_k^{(s)}, a_k^{(i)*}, ...\right]^T$. The electric field for both degenerate and non-degenerate cases can be written as:

$$\vec{E}_\omega(\vec{r},t) = e^{-i\omega t}\sum_m \Big(e^{-i\lambda_m t}\sum_k a_{k,m}^{(s)}|\vec{\psi}_k^{(a)}(\vec{r})\rangle + e^{+i\lambda_m^* t}\sum_k a_{k,m}^{(i)*}|\vec{\psi}_k^{(a)}(\vec{r})\rangle\Big) + c.c., \tag{19}$$

where $[\lambda_m]$ are the eigenvalues and $\vec{V}_m = [a_{k,m}^{(s,i)}]$ are the corresponding eigenvectors of the Hamiltonian ($\boldsymbol{\mathcal{H}}$) which define the signal/idler supermodes.

3. SECOND-HARMONIC GENERATION

We can implement the same approach for calculating the SHG in cavities. However, for SHG, we have to expand the second-harmonic mode into the eigenmodes of the cavity while the pump input at fundamental harmonic can be an embedded mode of the cavity. If we ignore the back conversion, the nonlinear dynamic for SHG process can be written as:

$$\sum_k\{\frac{\partial}{\partial t} - i\delta\omega^{(b_k)} + \frac{\alpha_k^{(b)}}{2}\}b_k(t)|\vec{\psi}_k^{(b)}(\vec{r})\rangle = \frac{i\omega}{n^2}\chi^{(2)}(2\omega,\omega,\omega)a^2(t)|\vec{\Psi}^{(a)}(\vec{r})\rangle^2. \tag{20}$$

By multiplying the both sides by $\langle\vec{\psi}_k^{(b)}|$. Eq. 20 is simplified to:

$$\frac{d}{dt}b_k = \left(i\delta\omega_k^{(b)} - \frac{\alpha_k^{(b)}}{2}\right)b_k + i2\tilde{\eta}_k^* a^2, \tag{21}$$

where $\tilde{\eta}_k = \omega\langle\mathcal{E}\frac{\chi^{(2)}}{n^2}\vec{\Psi}^{(a)^*}(\vec{r})^2\vec{\psi}_k^{(b)}(\vec{r})\rangle$. If we assume that the pump is constant ($a(t) = a_0$), the steady-state second-harmonic

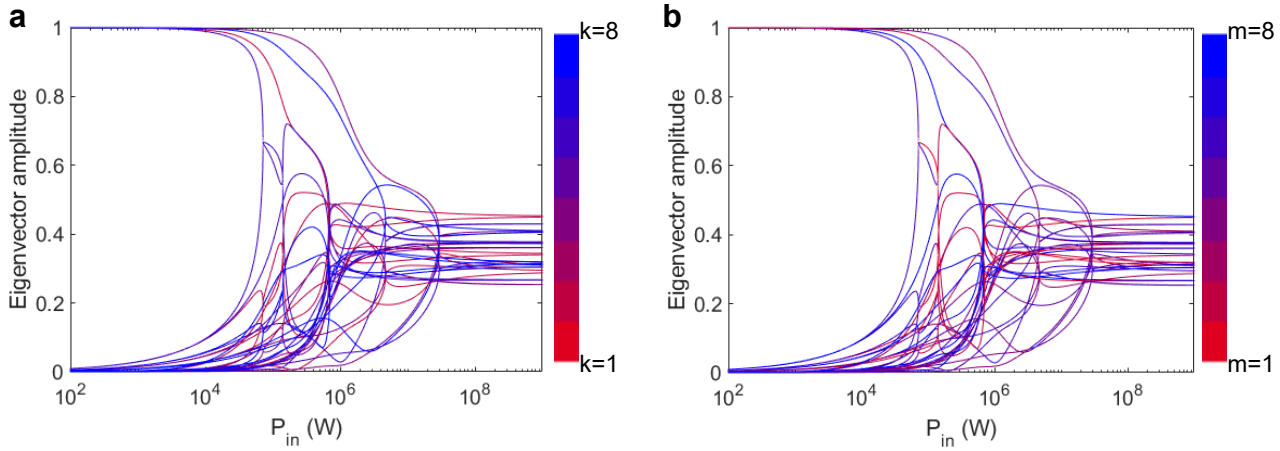

Fig. 3. Eigenvector amplitudes, $a^{(a)}_{k,m}$, for all eigenvalues. The structure is the same as that shown in Fig. 4 in the main text. **a** The color bar represents the mode number. **b** The color bar represents the eigenvalue number. It is seen that at low input power, each supermode corresponds to one eigenmode. However, as we approach the threshold the nonlinear coupling increases the contribution of other eigenmodes for all signal supermode.

generated power is:

$$|b_k|^2 = \frac{4\tilde{\eta}_k^2}{\frac{\alpha_k^{(b)^2}}{4} + \delta\omega_k^{(b)^2}} |a_0|^4 \tag{22}$$

If there is only one coupling channel between the input and the cavity mode at the fundamental frequency, the cavity mode amplitude can be written as the input power as:

$$|a_0|^2 = \frac{\alpha^{(a)}}{\frac{\alpha^{(a)^2}}{4} + \delta\omega^{(a)^2}} P_{\text{in}}, \tag{23}$$
$$|b_k|^2 = \frac{\alpha_k^{(b)}}{\frac{\alpha_k^{(b)^2}}{4} + \delta\omega_k^{(b)^2}} P_{\text{SHG},k}.$$

By inserting Eq. 23 in to Eq. 22, the second-harmonic power can be expressed as $P_{\text{SHG},k} = \epsilon_{\text{SHG},k} P_{\text{in}}^2$, where ϵ_{SHG} is the SHG efficiency in the unit of W^{-1} written as:

$$\epsilon_{\text{SHG},k} = \frac{4\tilde{\eta}_k^2 \alpha^{(a)^2}}{\alpha_k^{(b)} \left(\frac{\alpha^{(a)^2}}{4} + \delta\omega^{(a)^2}\right)^2}. \tag{24}$$

If the cavity is single mode at both the fundamental and second harmonic, $\tilde{\eta}_k = \eta_{kk}$. This allows us to connect the SHG efficiency to the nonlinear coupling coefficient. Hence, by knowing the linear response of the cavity and SHG efficiency, we can derive the OPO threshold by inserting Eq. 24 into Eq. 14:

$$P_{\text{th}} = \frac{4\alpha^{(a)^2}}{\alpha^{(b)^2} \epsilon_{\text{SHG}}} \left(\frac{\frac{\alpha^{(b)^2}}{4} + \delta\omega^{(b)^2}}{\frac{\alpha^{(a)^2}}{4} + \delta\omega^{(a)^2}} \right) \approx \frac{4}{\epsilon_{\text{SHG}}}. \tag{25}$$

4. OPO IN SPHERICAL DIELECTRIC PARTICLE

The nonlinear coupling matrix (Eq. 10) for the particle shown in Fig. 3 in the main text when the pump is at the resonant frequency of the 3$^{\text{rd}}$ magnetic mode is calculated as:

$$|\eta_{lk}| = 10^4 \times \begin{bmatrix} 0.5958 & 1.2898 & 1.1236 & 0.2458 \\ 1.2898 & 0.0454 & 0.1493 & 2.4897 \\ 1.1236 & 0.1493 & 0.4892 & 8.5686 \\ 0.2458 & 2.4897 & 8.5686 & 0.7508 \end{bmatrix} \tag{26}$$

The modes are ordered as: ED, EQ, MD, and MQ. The field overlap before the integration is shown in Fig. 1. It is seen that in the absence of the phase matching in wavelength-scale resonators, a strong local intensity of the overlap does not necessarily lead to a strong nonlinear coupling between two modes. This can also cause the off-diagonal terms to be stronger than the diagonal terms. If we ignore intermode coupling (off-diagonal terms), the threshold for these modes are: 3.99, 2783, 0.27, and 3.65 MW, respectively. However, due to the strong intermode coupling, which can be even stronger than the diagonal terms based on Eq. 26, the threshold is reduced 36-fold as shown in Fig. 3 in the main text.

For the wavelength-scale OPO reported in Fig. 6 of the main text, there are 9 eigenmodes involved. The resonant wavelength of these modes are: 2589, 1923, 1541, 1297, 3404, 2374, 1829, 1498, and 1273 nm. The first 4 modes are the electric modes and the last 5 modes are the magnetic modes. They are sorted from the lowest order to the highest order. The Q factor of these modes are 4, 19, 100, 520, 9, 37, 141, 600, and 2500, respectively. The

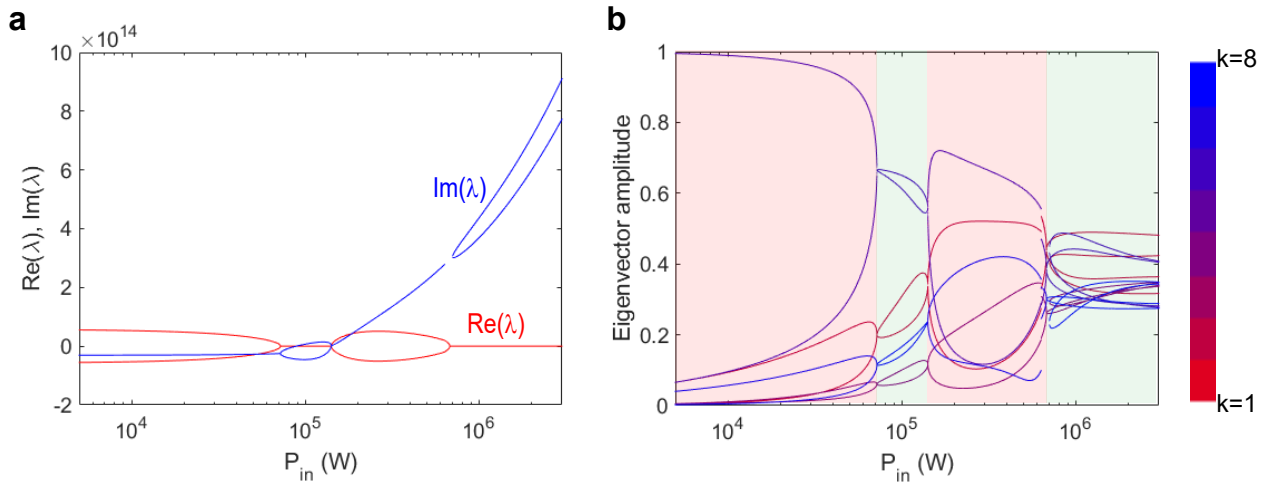

Fig. 4. Eigenvector amplitudes, $a^{(a)}_{k,m}$, for all eigenvalues. The structure is the same as that shown in Fig. 4 in the main text. **a** The real and the real parts of the two eigenvalues with the smallest real parts (as well as the largest imaginary parts for most of the input powers) **b** The eigenvectors for the corresponding supermodes. The degenerate and non-degenerate regions are shaded as green and red, respectively. The eigenvalues as well as the eigenvectors of the two modes coalesce when there is a transition from degenerate to non-degenerate cases and vice versa.

nonlinear coupling term for the pump excitation at 1110 nm is:

$$|\eta_{lk}| = 10^4 \times \tag{27}$$

$$\begin{bmatrix}
0.2 & 0.6 & 0.6 & 0.5 & 0.1 & 0.6 & 0.5 & 4.4 & 0.1 \\
0.6 & 0.5 & 0.3 & 2.7 & 0.5 & 0.8 & 7.0 & 0.5 & 37.9 \\
0.6 & 0.3 & 2.7 & 0.1 & 0.9 & 8.8 & 1.1 & 18.7 & 0.6 \\
0.5 & 2.7 & 0.1 & 14.2 & 8.2 & 1.1 & 5.9 & 1.2 & 18.5 \\
0.1 & 0.5 & 0.9 & 8.2 & 0.5 & 0.2 & 0.8 & 0.1 & 118 \\
0.6 & 0.8 & 8.8 & 1.1 & 0.2 & 0.6 & 0.5 & 146 & 0.5 \\
0.5 & 7.0 & 1.1 & 5.9 & 0.8 & 0.5 & 149 & 0.3 & 33.1 \\
4.4 & 0.5 & 18.7 & 1.2 & 0.1 & 146 & 0.3 & 36.4 & 0.1 \\
0.1 & 37.9 & 0.6 & 18.5 & 118 & 0.5 & 33.1 & 0.1 & 22.8
\end{bmatrix}$$

The nonlinear coupling term for the pump excitation at 1125 nm is:

$$|\eta_{lk}| = 10^4 \times \tag{28}$$

$$\begin{bmatrix}
0.4 & 0.6 & 6.5 & 0.6 & 0.1 & 1.1 & 0.7 & 8.1 & 0.2 \\
0.6 & 5.8 & 0.3 & 7.0 & 2.5 & 1.0 & 6.3 & 0.7 & 6.7 \\
6.5 & 0.3 & 8.3 & 0.1 & 1.1 & 9.3 & 1.1 & 8.7 & 0.8 \\
0.6 & 7.0 & 0.1 & 2.7 & 15.5 & 1.2 & 12.5 & 1.4 & 9.2 \\
0.1 & 2.5 & 1.1 & 15.5 & 0.3 & 0.3 & 7.2 & 0.1 & 2.6 \\
1.1 & 1.0 & 9.3 & 1.2 & 0.3 & 7.3 & 0.6 & 1.9 & 0.5 \\
0.7 & 6.3 & 1.1 & 12.5 & 7.2 & 0.6 & 1.8 & 0.5 & 1.5 \\
8.1 & 0.7 & 8.7 & 1.4 & 0.1 & 1.9 & 0.5 & 2.0 & 0.3 \\
0.2 & 6.7 & 0.8 & 9.2 & 2.6 & 0.5 & 1.5 & 0.3 & 3.0
\end{bmatrix}$$

The eigenvalues at these two wavelengths are shown in Fig. 2. It is seen that at the threshold, since the signal and idler frequency separation is large, the parametric gain is low. However, when a phase transition from non-degenerate to degenerate case occurs, the gain boosts rapidly.

5. THE EVOLUTION OF SUPERMODES

The supermodes are the eigenvectors of $\mathcal{H}(b)$. The eigenvectors for all eigenvalues are displayed in Fig. 3. The odd and even numbers correspond to the signal and idler modes, respectively. The eigenvectors, $a^{(a)}_{k,m}$, corresponding to the eigenvalues illustrated in Fig. 4 in the main text is displayed in Fig. 4.

6. QUASI-NORMAL MODE FORMULATION

The expansion of fields in a 3D resonator to multi-polar Mie resonances, which we have used in the main text, satisfies orthogonality and completeness only for spherical and non-dispersive structures. Hence, it cannot be applied to the general case of a resonator with an arbitrary shape. For a dispersive material, the conventional form of source-free Maxwell's equations cannot be written as a standard linear eigenproblem [1]. Recently, Lorentz reciprocity theorem [4, 5] has been proposed to find the linear response of arbitrarily shaped plasmonic and dielectric resonators composed of a material with single-pole Lorentz dispersion in the form of $\varepsilon(\omega) = \varepsilon_\infty \left(1 - \frac{\omega_p^2}{\omega^2 - \omega_0^2 + i\gamma\omega}\right)$. In this approach, two auxiliary fields are introduced: the polarization, $\vec{P} = -\varepsilon_\infty \left(1 - \frac{\omega_p^2}{\omega^2 - \omega_0^2 + i\gamma\omega}\right) \vec{E}$, and the current density, $\vec{J} = -i\omega\vec{P}$, to reformulate the Maxwell's equation in a linear

form [4]:

$$\begin{bmatrix} 0 & -i\mu_0^{-1}\nabla\times & 0 & 0 \\ i\varepsilon_\infty^{-1}\nabla\times & 0 & 0 & -i\varepsilon_\infty^{-1} \\ 0 & 0 & 0 & i \\ 0 & i\omega_p^2\varepsilon_\infty & -i\omega_0^2 & -i\gamma \end{bmatrix} \begin{bmatrix} \vec{E}_m \\ \vec{H}_m \\ \vec{P}_m \\ \vec{J}_m \end{bmatrix} = \omega_m \begin{bmatrix} \vec{E}_m \\ \vec{H}_m \\ \vec{P}_m \\ \vec{J}_m \end{bmatrix}. \tag{29}$$

By applying proper boundary conditions [1], this approach can be used to precisely find quasi-normal modes for an arbitrarily shaped 3D resonator. Beside the quasi-normal modes, this approach can find a continuum of background modes which depends on the boundary conditions, and can form a complete basis combined with quasi-normal modes.

Because of the low Q nature of the background mode, their contribution on the OPO threshold is negligible. However, they can change the field distribution of supermodes and their spectral response above the threshold. The connection between the quasi-normal modes and the density of states, $\rho(\omega)$, has been discussed in previous works [5, 6].

If we have a continuum of states, the summation in Eq. 17 is converted to an integral form as:

$$\frac{d}{dt}a_l^{(s)} = \left(i\delta\omega_l^{(a)} - \frac{\alpha_l^{(a)}}{2} \right) a_l^{(s)} + ib \int d\omega \rho(\omega) \eta_{l\omega} a_\omega^{(i)*}. \tag{30}$$

Since the effect of low-Q background modes are negligible, to simplify the numerical calculations, we can discretize Eq. 30 around the quasi-normal modes:

$$\frac{d}{dt}a_l^{(s)} = \left(i\delta\omega_l^{(a)} - \frac{\alpha_l^{(a)}}{2} \right) a_l^{(s)} + ib \sum_k \int d\omega \rho_k(\omega) \eta_{lk} a_k^{(i)*}, \tag{31}$$

where $\rho_k(\omega)$ is the density of states around the resonant frequency of the k^{th} quasi-normal mode of the resonator.

REFERENCES

1. W. Yan, R. Faggiani, and P. Lalanne, "Rigorous modal analysis of plasmonic nanoresonators," Phys. Rev. B **97**, 205422 (2018).
2. H. A. Haus, *Waves and fields in optoelectronics* (Prentice-Hall,, 1984).
3. A. Rodriguez, M. Soljačić, J. D. Joannopoulos, and S. G. Johnson, "χ (2) and χ (3) harmonic generation at a critical power in inhomogeneous doubly resonant cavities," Opt. express **15**, 7303–7318 (2007).
4. P. Lalanne, W. Yan, K. Vynck, C. Sauvan, and J.-P. Hugonin, "Light interaction with photonic and plasmonic resonances," Laser & Photonics Rev. **12**, 1700113 (2018).
5. C. Sauvan, J.-P. Hugonin, I. Maksymov, and P. Lalanne, "Theory of the spontaneous optical emission of nanosize photonic and plasmon resonators," Phys. Rev. Lett. **110**, 237401 (2013).
6. E. Muljarov and W. Langbein, "Exact mode volume and purcell factor of open optical systems," Phys. Rev. B **94**, 235438 (2016).